

Human Movement Forecasting with Loose Clothing

Tianchen Shen¹, Irene Di Giulio² and Matthew Howard¹

Abstract—Human motion prediction and trajectory forecasting are essential in human motion analysis. Nowadays, sensors can be seamlessly integrated into clothing using cutting-edge electronic textile (e-textile) technology, allowing long-term recording of human movements outside the laboratory. Motivated by the recent findings that clothing-attached sensors can achieve *higher* activity recognition accuracy than body-attached sensors. This work investigates the performance of human motion prediction using clothing-attached sensors compared with body-attached sensors. It reports experiments in which statistical models learnt from the movement of loose clothing are used to predict motion patterns of the body of robotically simulated and real human behaviours. Counter-intuitively, the results show that fabric-attached sensors can have *better* motion prediction performance than rigid-attached sensors. Specifically, The fabric-attached sensor can *improve* the accuracy up to 40% and requires up to 80% *less* duration of the past trajectory to achieve high prediction accuracy (*i.e.*, 95%) compared to the rigid-attached sensor.

I. INTRODUCTION

Human motion prediction and trajectory forecasting are crucial for understanding human motion in various research areas [1], ranging from human-robot interaction (*e.g.*, service robots [2]), human-robot collaboration in manufacturing [3] to rehabilitation devices (*e.g.*, exoskeleton robots [4]). With the latest e-textile technology, sensors can be embedded in clothing [5], ensuring comfortable and unobtrusive wear for users. This allows for the recording of human movement outside the laboratory for long periods [6].

However, a challenge in recording human movement using e-textile is the potential inclusion of motion artefacts caused by the movement of clothing with respect to the body. Many different approaches have been used to address this issue. For example, (i) sensors have been tightly attached to the body using tape [7], [8], (ii) attached to tight-fitting clothing [9] or (iii) statistical machine learning/signal processing methods have been employed to reduce artefacts [10]–[12]. However, an increasing body of work [13]–[17] suggests fabric motion could in fact be *useful* for human motion recognition. Inspired by this, this paper focuses on *forecasting human motion patterns from loose clothing*.

Fig. 1 illustrates the concept of the approach taken in this paper. Future movement (dashed line and shaded area) is

This work was supported by King’s College London, the China Scholarship Council and Engineering and Physical Sciences Research Council (EP/M507222/1). For the purpose of open access, the authors have applied a Creative Commons Attribution (CC BY) license to any Accepted Manuscript version arising.

¹Tianchen Shen (tianchen.shen@kcl.ac.uk) and Matthew Howard are with the Centre for Robotics Research, Department of Engineering, King’s College London, UK.

²Irene Di Giulio is with Centre for Human and Applied Physiological Sciences, King’s College London, UK.

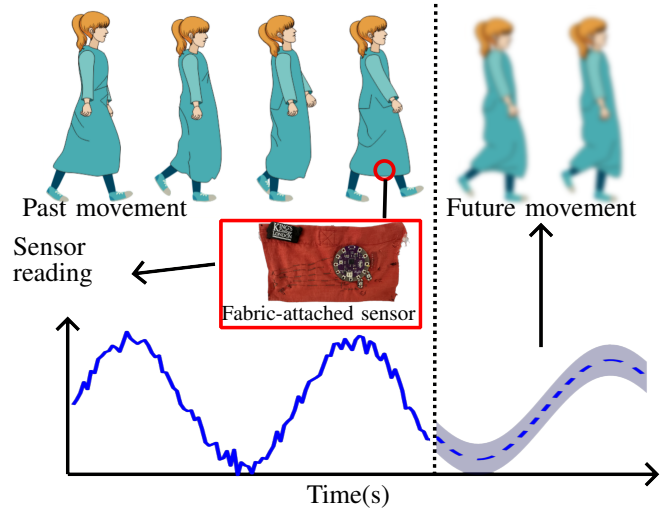


Fig. 1: Illustration of human movement forecasting. The future human movement (dashed line and shaded area) is forecasted based on the past movement of the clothing-attached sensor (solid line).

forecasted based on the motion prediction made using the movement of the clothing during the past period collected from the clothing-attached sensor (solid line)¹.

This paper solves human motion prediction and trajectory forecasting problems using Left-to-Right Hidden Markov models (LR-HMMs). The proposed approach works by eliciting the movement class from the LR-HMMs, then using those same LR-HMMs to forecast the movement. The experimental results suggest models trained on data from clothing-attached sensors can lead to *higher* prediction accuracy and require *less* time to achieve high accuracy compared to those trained on data from rigidly-attached sensors. Once the correct motion is predicted, the future trajectory can be forecasted using the past trajectory recorded by a rigid-attached sensor. Furthermore, the statistical distance (*i.e.*, cross-fitness distance) between LR-HMMs is used to estimate discrimination information and understand this counterintuitive phenomenon.

II. PROBLEM DEFINITION

The approach proposed in this paper aims to forecast future human body movement $\vec{Y}^r = [y_{v+1}^r, y_{v+2}^r \dots y_V^r]$

¹In this paper, the term “motion prediction” is used to refer to the classification of past movements (*e.g.*, distinguishing between walking and running), while “motion forecasting” refers to predicting the future time course of a movement *e.g.*, the positions of a point of the body over time).

based on the movement of clothing $\mathbf{Y}^f = [y_1^f, y_2^f \dots y_v^f]$ using a statistical model trained on past movements.

The latter is trained on data in which body and clothing-attached sensors are used to simultaneously record movement for \mathcal{V} time steps with \mathcal{M} features as a person performs \mathcal{K} repetitions of a given motion of a predefined class. For example, the sensors may record the multi-dimensional orientations of the human body and clothing when a person is walking. Each movement recorded consists of \mathcal{V} sensor readings, *i.e.*, $\mathbf{Y}_k = [y_1, y_2 \dots y_{\mathcal{V}}] \in \mathbb{R}^{\mathcal{M} \times \mathcal{V}}$, and is assumed to belong to one of a finite, discrete set of motions/classes (*e.g.*, walking, running)². The complete set of recordings consist of the body- $\mathbf{X}^r = [\mathbf{Y}_1^r, \mathbf{Y}_2^r, \dots, \mathbf{Y}_{\mathcal{K}}^r] \in \mathbb{R}^{\mathcal{M} \times \mathcal{K} \times \mathcal{V}}$ and the clothing-attached sensor readings $\mathbf{X}^f = [\mathbf{Y}_1^f, \mathbf{Y}_2^f, \dots, \mathbf{Y}_{\mathcal{K}}^f] \in \mathbb{R}^{\mathcal{M} \times \mathcal{K} \times \mathcal{V}}$. At deployment (*i.e.*, once the model has been trained) it is assumed that *no further direct sensing of the body is available*, *i.e.*, motion classification and forecasting rely solely on data from fabric-attached sensors.

III. METHODOLOGY

A. Left-to-Right Hidden Markov model parameter set up

An Hidden Markov model (HMM) is used to predict the motion of the past human body \mathbf{Y}^r and the clothing movement \mathbf{Y}^f and formulate the probabilistic trajectory model using human body movement \mathbf{X}^r . HMMs are suitable for modelling time series data in a wide range of applications [18]. This is because they are easy to build and manipulate, and optimal algorithms exist to train and score them, such as the forward algorithm and the Viterbi algorithm [19].

The following introduces the set-up of the HMMs [20]. Consider an \mathcal{N} -state Markov chain where the individual states are denoted as $S = \{s_1, s_2, \dots, s_{\mathcal{N}}\}$. The sequence of states that follows the chronological order of the sensor readings is defined as the most likely state sequence, denoted as $\mathcal{Q} = \{q_1, q_2, \dots, q_{\mathcal{V}}\}$. The most likely state at time step v is q_v . The estimated value in the future trajectory is in the continuous measurement space.

The transitions between these individual states are defined by the transition probability matrix $\mathbf{A} = \{a_{ij}\}$, whose elements are

$$a_{ij} = P(q_v = s_j | q_{v-1} = s_i), \quad 1 \leq i, j \leq \mathcal{N}. \quad (1)$$

a_{ij} represents the probability of transitioning to state s_j at time step v , conditional on being in state s_i at time step $v - 1$ ³.

The emission probability, denoted as \mathbf{B} , is defined as follows: $\mathbf{b}_i(\mathbf{Y}_v)$ represents the probability of an individual state s_i given sensor readings \mathbf{Y}_v at time step v . It is defined by the Gaussian probability density function:

$$\mathbf{b}_i(\mathbf{Y}_v) = P(\mathbf{Y}_v | q_v = s_i) = \mathcal{N}(\mu_i, \Sigma_i), \quad 1 \leq i \leq \mathcal{N}. \quad (2)$$

²Throughout the paper, without loss of generality, all prediction tasks are assumed to be binary.

³As the sensor reading progresses with each time step, the probability of transitioning to state s_j at time v , given that it was in state s_i at time step $v - 1$, is much higher than remaining in state s_i at time step v . (*i.e.*, $a_{ij} \gg a_{ii}$).

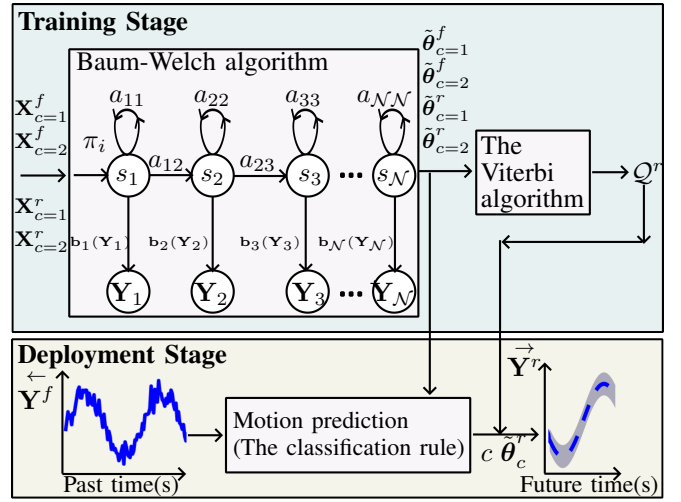


Fig. 2: The framework for motion prediction and trajectory forecasting based on LR-HMM. The future human movement \mathbf{Y}^r (dashed line and shaded area) is forecasted based on the prediction label c of the past clothing movement \mathbf{Y}^f (solid line) and the probability trajectory model $\tilde{\theta}_c^r$ formulated by body movement using the Baum-Welch algorithm and the Viterbi algorithm.

The initial (*i.e.*, $v = 1$) state distribution is

$$\pi_i = P(q_1 = s_i), \quad 1 \leq i \leq \mathcal{N}. \quad (3)$$

The number of individual states is set to be equal to the number of time steps in each observation trajectory (*i.e.*, $\mathcal{N} = \mathcal{V}$). This implies that each state represents a specific time step in observation. This choice is designed to maximise the performance of the forecasting. This type of HMM is also known as a Left-to-Right Hidden Markov model (LR-HMM) [21]. A compact notation of the LR-HMM parameters is $\theta = \{\pi, \mathbf{A}, \mathbf{B}\}$.

B. Left-to-Right Hidden Markov model parameter estimation

The Baum-Welch algorithm is used to estimate the LR-HMM parameters $\tilde{\theta}_{c=1}^r$, $\tilde{\theta}_{c=2}^r$, $\tilde{\theta}_{c=1}^f$ and $\tilde{\theta}_{c=2}^f$, given sensor readings $\mathbf{X}_{c=1}^r$, $\mathbf{X}_{c=2}^r$, $\mathbf{X}_{c=1}^f$, $\mathbf{X}_{c=2}^f$.

This method is used to adjust the LR-HMM to maximise $P(\mathbf{X}|\theta)$ *i.e.*,

$$\tilde{\theta} = \underset{\theta}{\operatorname{argmax}} \sum_{k=1}^{\mathcal{K}} \log P(\mathbf{Y}_k | \theta). \quad (4)$$

See [22] for details.

C. Motion prediction

The classification rule introduced in [23] is used to make a prediction using the rigid-attached sensor and the fabric-attached sensor. This compares likelihoods based on two LR-HMM parameters and the past trajectory. *i.e.*,

$$\begin{aligned} c &= \underset{c}{\operatorname{argmax}} \log P(\mathbf{Y}^f | \tilde{\theta}_c^f), \quad c \in \{1, 2\} \\ c &= \underset{c}{\operatorname{argmax}} \log P(\mathbf{Y}^r | \tilde{\theta}_c^r), \quad c \in \{1, 2\} \end{aligned} \quad (5)$$

The forward algorithm, as described in [22], is used to compute the likelihoods of the past trajectory given LR-HMM parameters.

D. Trajectory forecasting

In this paper, each individual state is set to correspond to a specific time step in the observation trajectory. However, it is not explicitly determined which individual state in the estimated LR-HMM corresponds to which time step in the observation trajectory. Formulating the probabilistic trajectory model requires finding which individual state corresponds to each time step of the observation trajectory. Therefore, the most likely state sequence \mathcal{Q}^r needs to be solved using the Viterbi algorithm, as described in [22]. After that, the probability density function of each individual state given the rigid-attached sensor's reading \mathbf{Y}_v^r at each time step v (i.e., emission probability \mathbf{B}) and the most likely state sequence \mathcal{Q}^r can be used to form the probabilistic trajectory model (i.e., $\mathbf{b}_{q_1}(\mathbf{Y}_1^r), \mathbf{b}_{q_2}(\mathbf{Y}_2^r), \mathbf{b}_{q_3}(\mathbf{Y}_3^r) \dots \mathbf{b}_{q_v}(\mathbf{Y}_v^r)$).

To conclude, in the training stage, given the observations (i.e., rigid and fabric-attached sensor readings) of two classes of movements $\mathbf{X}_{c=1}^f, \mathbf{X}_{c=2}^f, \mathbf{X}_{c=1}^r$ and $\mathbf{X}_{c=2}^r$, the LR-HMMs parameters $\tilde{\theta}_{c=1}^f, \tilde{\theta}_{c=2}^f, \tilde{\theta}_{c=1}^r$ and $\tilde{\theta}_{c=2}^r$ are estimated using the Baum–Welch algorithm, the most likely state sequence \mathcal{Q}^r is estimated using the Viterbi algorithm to formulate the probabilistic trajectory model of the rigid movement.

In the deployment stage, the past fabric movement \mathbf{Y}^f (solid line, see Fig. 2) is then used to recognise the movement (i.e., $c = 1$ or $c = 2$ is determined) using the classification rule, and based on this, the probabilistic trajectory model of the rigid movement is used to forecast the future rigid movement $\hat{\mathbf{Y}}^r$ (dashed line and shaded area, see Fig. 2).

IV. EXPERIMENTS

A. Case Study 1: Linear and curved point-to-point movements

The aim of the first evaluation is to estimate the performance of the proposed approach in recognising and forecasting simple movement patterns. For this, in the first case study, a robotic simulation of human movement is used, in order to eliminate variability in the motion pattern that may confound the experimental results (real human movement is addressed in §IV-B below). To this end, a robot arm with a piece of fabric attached is used as a proxy for the human arm, to collect reliable and repeatable movements.

1) *Materials and Methods*: KUKA's LBR iiwa robot arm (KUKA, Germany) is used to execute PTP movement encompassing both linear (SLIN) and curved (SCIRC) motion, using KUKA Sunrise.OS 1.11. Fig. 3(a) shows the experimental set up, comprising a 30 cm × 5 cm strip of woven cotton fabric attached at the end effector of the robot arm. Three sensors (NDI Aurora Magnetic Tracking device, NDI, Canada) are mounted on this fabric strip to record positions and orientations synchronously (both are in three dimensions) at $f_s = 40$ Hz. The sensors are attached along the length of the fabric (i) 20 cm (F_2), (ii) 30 cm

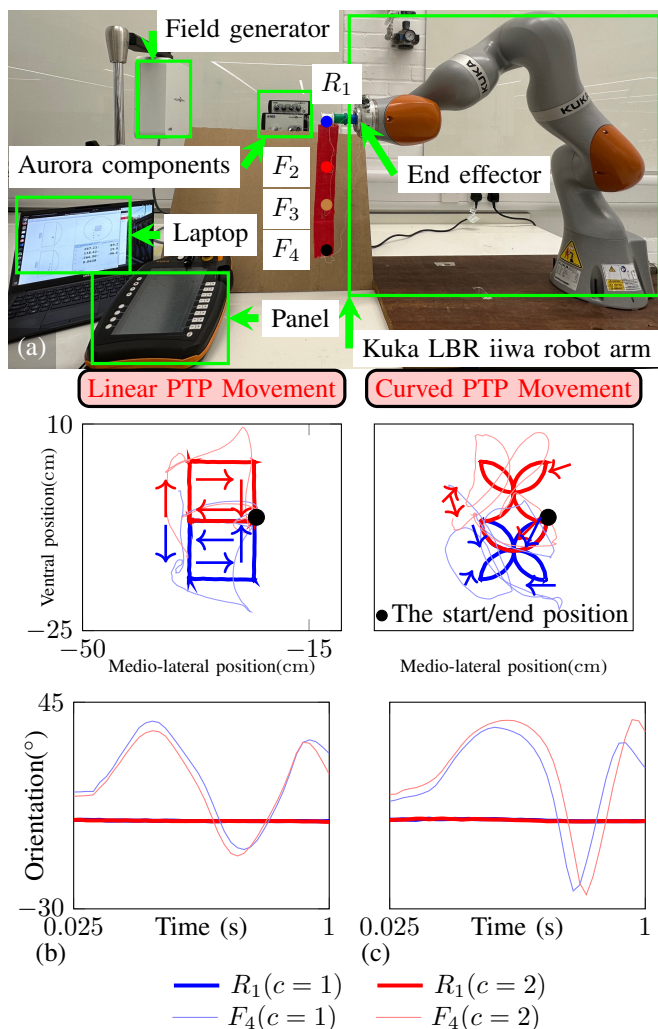


Fig. 3: (a) Experimental setup. The robot arm with a piece of fabric attached to the end effector. The actual moving trajectories and the longitudinal/X-axis (roll) orientation of the rigid-attached sensor and the fabric-attached sensor during (b) linear and (c) curved point-to-point (PTP) movement. Note that the variations of rigid movements in both types of movements are less obvious.

(F_3) and (iii) 40 cm from the fulcrum (F_4) (i.e., at the tip of the fabric). It is helpful to understand how different sensor placements on the piece of the fabric influence motion prediction accuracy. A sensor (R_1) is rigidly attached to the end effector of the robot arm at the fabric attachment point. The end effector of the robot arm moves at 2.25 cm s^{-1} in linear and curved PTP movements. The trajectory of the rigid-attached sensor (R_1 thick and dark line) and the fabric-attached sensor (F_4 thin and light line) during linear and curved PTP movements are shown in Fig. 3(b) and (c), respectively. The colours red and blue represent two classes of movement to be predicted. In both types of movement, the variations in rigid movements are less pronounced because the robot arm moves very smoothly. With this set up, $\mathcal{K} = 50$

trajectories of length $T = 3.5$ s at each class of movement are recorded ($\mathcal{V} = f_s \times T = 40 \times 3.5 = 140$ data points). Motion predictions are made based on the orientations (*i.e.*, $\mathcal{M} = 3$) of each sensor's readings $\mathbf{X}_{c=1}^r$, $\mathbf{X}_{c=2}^r$, $\mathbf{X}_{c=1}^f$ and $\mathbf{X}_{c=2}^f$ since the widely used Inertial Measurement Unit (IMU)s can also receive orientation data. 49 trajectories are randomly chosen from each class of movement of each sensor used to train the separate LR-HMMs $\tilde{\theta}_{c=1}^r$, $\tilde{\theta}_{c=2}^r$, $\tilde{\theta}_{c=1}^f$ and $\tilde{\theta}_{c=2}^f$. The remaining trajectories are reserved for testing purposes. Motion prediction is decided using equation (5). The above-described process is repeated 100 times. The prediction accuracy is calculated as

$$\text{Prediction accuracy} = \frac{\text{number of correct predictions}}{\text{total number of predictions}}. \quad (6)$$

The motion prediction accuracy of each sensor is evaluated separately. Once the label of the past movement is predicted, the LR-HMM trained using the positions of sensors R_1 and the Viterbi algorithm is used to forecast the future robot movement. To understand the reason why fabric-attached sensors have higher motion prediction accuracy, the information content of the rigid and fabric movement is investigated. The statistical distance between LR-HMMs given two categories of movements is computed as a measure of discrimination information between two classes of HMMs [24]. The cross-fitness distance of rigid movements D^r and fabric movements D^f is computed as proposed in [25]. The formula is shown below:

$$\begin{aligned} D^r &= \log P(\mathbf{X}_{c=1}^r | \tilde{\theta}_{c=1}^r) + \log P(\mathbf{X}_{c=2}^r | \tilde{\theta}_{c=2}^r) \\ &\quad - \log P(\mathbf{X}_{c=1}^r | \tilde{\theta}_{c=2}^r) - \log P(\mathbf{X}_{c=2}^r | \tilde{\theta}_{c=1}^r), \\ D^f &= \log P(\mathbf{X}_{c=1}^f | \tilde{\theta}_{c=1}^f) + \log P(\mathbf{X}_{c=2}^f | \tilde{\theta}_{c=2}^f) \\ &\quad - \log P(\mathbf{X}_{c=1}^f | \tilde{\theta}_{c=2}^f) - \log P(\mathbf{X}_{c=2}^f | \tilde{\theta}_{c=1}^f). \end{aligned} \quad (7)$$

2) *Results*: Fig. 4(a) and (b) illustrate the motion prediction accuracy and the cross-fitness distance between two classes of movement for linear and curved PTP movements, respectively. The accuracy of the clothing-attached sensors is significantly higher than that of the rigidly-attached sensors in both types of movements. The accuracy using fabric movement can increase by around 40% and requires 80% less time length of past movement to get 95% prediction accuracy compared with using rigid movement. The placement of fabric-attached sensors does not appear to have an obvious effect on motion prediction accuracy. The cross-fitness distance of the fabric-attached sensor is higher than the rigid-attached sensor. This indicates that clothing movement provides additional information to simplify the prediction task. Fig. 4(c) and (d) show the forecasted movement (dashed line and shaded area) given the past movement (solid line) time step one ($v = 1$, $t = 0$) to $t = 1$ s when the robot arm performs linear and curved PTP movements, respectively. The motion prediction accuracy using the orientations of rigid and fabric movement at that time is also shown. The motion prediction accuracy of using sensor F_4 is higher than using sensor R_1 . The dashed line is the future trajectory with the highest probability (*i.e.*, the mean of each $\mathbf{b}_i(\mathbf{Y}_v)$).

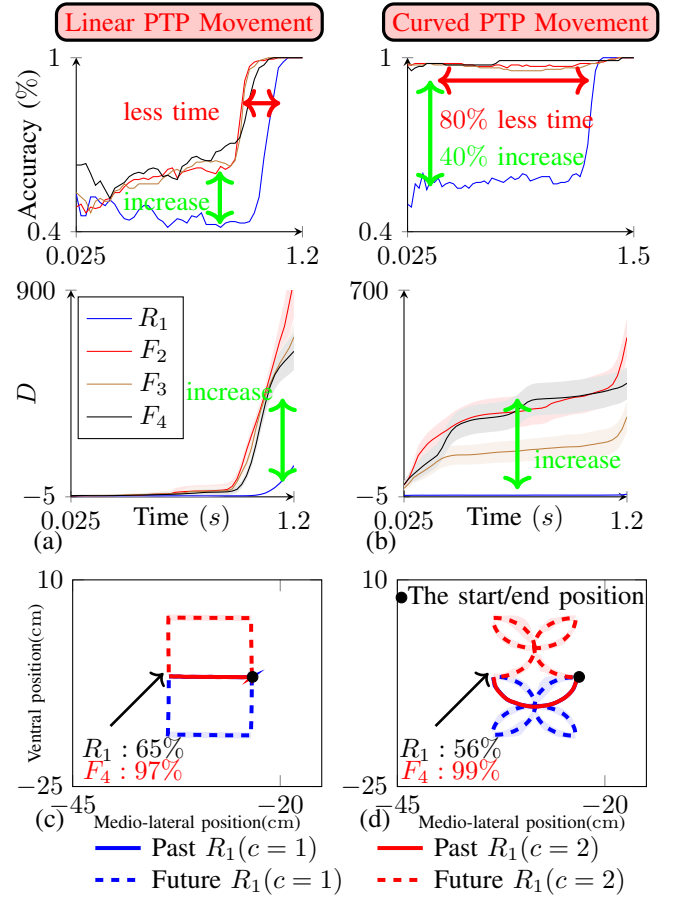


Fig. 4: The accuracy of motion prediction and the cross-fitness distance from the first time step to 1.2s in the contexts of (a) linear and (b) curved PTP movements. Reported are the mean value \pm s.d./5. Panels (c) and (d) show the forecasting of linear and curved PTP movements, respectively. The future robot movement is forecasted (dashed line) based on 1 s of past movement (solid line). The future trajectory shown is the mean value (dashed line) \pm s.d. \times 5 (shaded area).

The shaded area represents probability (*i.e.*, the standard derivation of each $\mathbf{b}_i(\mathbf{Y}_v)$). Specifically, the further away from the dashed line, the less likely the trajectory is to occur. The thick and light lines are sensor R_1 and F_4 movement, respectively.

B. Case Study 2: Human motion prediction

The second evaluation aims to test the performance of the proposed approach on forecasting real human motion⁴. For this, a human reaching motion is chosen as it is a common daily activity. Specifically, the scenario considered here consists of reaching to press one of a set of buttons, and the task is to predict which button the person intends to hit *before the button is pressed*.

⁴The experiments reported here were conducted with the ethical approval of King's College London, UK: MRPP-23/24-40031.

1) *Materials and Methods*: The experimental setup includes five buttons and five LED lights. The white button marks the hand’s starting position, while the other four buttons represent different target positions. The distance between each target button and the start button is 45 cm, ensuring uniform travel durations to reach each target. The angle between two adjacent target buttons is 5 degrees, so all target buttons are positioned on an arc centred on the start button. To deactivate a target LED light, the participant must press the button of the corresponding colour. Fig. 5(a) shows the experimental setup.

The participant was provided with an information sheet and signed a consent form before visiting the laboratory. Before data collection, the participant’s sitting position is standardised. The distance between the centre of the shoulder joint and the reference point (see Fig. 5(a)) is 70% of the participant’s arm length. The sleeve is adjusted to ensure the cuff is aligned flush with the wrist using tape. All data collection is conducted exclusively in an audio-visual isolated room. To familiarise the participant with the movement, a brief video is presented to demonstrate the specific movements to be performed.

The participant is asked to remove or roll up the sleeve of any clothing on their arms and to wear an instrumented shirt (100% woven cotton) with one sensor (denoted as F) attached to the cuff of the right-side sleeve (with a maximum possible displacement from the wrist of ± 10 cm) and another sensor attached near the unciform bone (denoted as R). The participant is asked to clench the dominant hand into a fist and use the thumb to fully press the start button, which turns off the corresponding LED light. Subsequently, the subject reaches directly for and presses the button corresponding to the randomly illuminated LED within 2.5s. The participant’s hand then returns to the starting position, awaiting the re-illumination of the LED light. This procedure is repeated 40 times, with each target LED illuminating 10 times per block. The experiment involved a total of 5 blocks. The release times of all buttons are recorded.

Following this procedure, the healthy male participant is invited to this experiment. As a result, an equal number of samples (50 for each target button) are recorded. The start time index of each trajectory is identified when the change in the horizontal dimension of wrist-attached sensor movement exceeds 10 mm. The length of each hand-reaching trajectory is determined by the minimal time interval between the release of the start button and the target buttons (*i.e.*, $T = 0.75$ s). Each trajectory occurring within this designated time interval, initiating from each start time index, is retained for further analysis ($\mathcal{V} = f_s \times T = 0.75 \times 40 = 30$ data points). Human motion prediction and trajectory forecasting are solved according to the methods outlined in §III.

2) *Results*: Fig. 5 (a) and (b) show the motion prediction accuracies and the cross-fitness distance between buttons 1 and 2, buttons 2 and 3 and buttons 3 and 4, respectively. The motion prediction accuracy of the sleeve-attached sensor is higher than the wrist-attached sensor, and the former requires a shorter duration to attain high accuracy. During

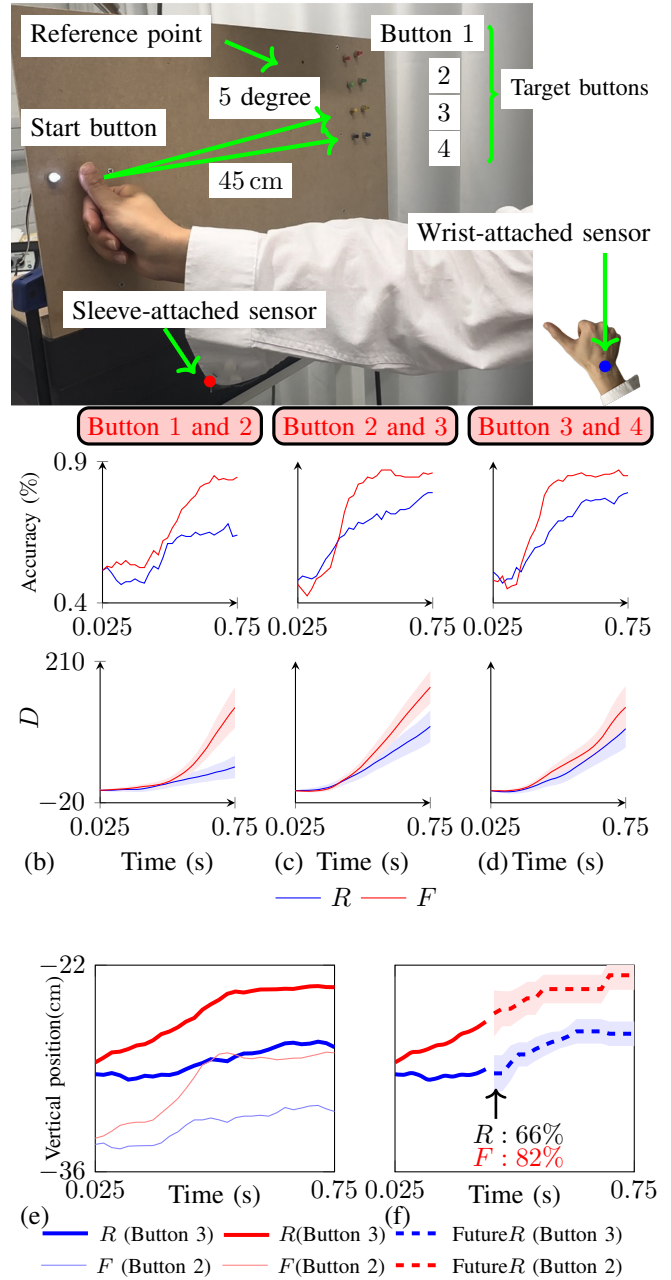


Fig. 5: (a) Experimental setup. The participant presses a start button and then reaches for one of the target buttons. The sensors are attached to the wrist and the tip of the sleeve. The motion prediction accuracy and the cross-fitness distance between (b) button 1 and 2, (c) button 2 and 3 and (d) button 3 and 4 given various durations of the past movement. Reported are the mean value \pm s.d/5. (e) The vertical position of the sensor’s movement when the human arm is reaching button 2 and button 3. (f) The future movement of the human body (dashed line and shaded area) is predicted based on their past movement (solid line) from the initial time step up to 0.6s. The future trajectory shown is the mean value (dashed line) \pm s.d \times 5 (shaded area). The motion prediction accuracies using the past movement until 1 s recorded by sensor R_1 and F_4 are shown.

the beginning of the human reaching movement, the accuracy of the sleeve-attached sensor does not exhibit a significant increase. This may be attributed to the relatively low arm moving speed at the beginning of the movement. The cross-fitness distance of the sleeve-attached sensor is higher than the wrist-attached sensor. This shows the sleeve movement has additional information to simplify the prediction task. Fig. 5(f) shows the future human movement (dashed line) forecasted based on the past sleeve movement given data from time step one ($v = 1, t = 0$) to $t = 0.3$ s.

V. DISCUSSION

This work compares the motion prediction performance between using body-attached and clothing-attached sensors. Motion prediction is an important step before forecasting the future human movement using the body-attached sensor. Counter-intuitively, (i) the performance of motion prediction improves using clothing movement and (ii) clothing-attached sensors require a shorter duration of the past trajectory to achieve high accuracy. (iii) This phenomenon is explained by computing the statistical distance (*i.e.*, cross-fitness distance). Motion artefacts can increase statistical distance which contains more discrimination information and makes it easier to distinguish two categories of movements.

This finding suggests that the sensor should be attached to loose clothing that can more effectively address the motion prediction problem using the body-attached sensor. Motion prediction in this study is primarily based on measurements of the orientation of the fabric since this is the primary sensing modality available from accelerometers/IMUs used in most wearable motion capture technologies, and therefore the findings may have widespread applications.

In turn, this finding could have implications for many applications in robotics and automation. Such as prostheses [26], and human-robot collaboration (*e.g.*, assist the worker in the industry [27], the mobile robot could assist the staff in the retail environment [28]). Future work may explore more complex human movements, such as multi-joint upper limb movement or gait.

REFERENCES

- [1] P. Kothari, S. Kreiss, and A. Alahi, "Human Trajectory Forecasting in Crowds: A Deep Learning Perspective," *IEEE TITS*, vol. 23, no. 7, pp. 7386–7400, 2021.
- [2] A. Rudenko, L. Palmieri, M. Herman, K. M. Kitani, D. M. Gavrila, and K. O. Arras, "Human Motion Trajectory Prediction: A Survey," *IJRR*, vol. 39, no. 8, pp. 895–935, 2020.
- [3] Z. Liu, Q. Liu, W. Xu, Z. Liu, Z. Zhou, and J. Chen, "Deep Learning-based Human Motion Prediction considering Context Awareness for Human-Robot Collaboration in Manufacturing," *procedia cirp*, vol. 83, pp. 272–278, 2019.
- [4] S. Qiu, W. Guo, D. Caldwell, and F. Chen, "Exoskeleton Online Learning and Estimation of Human Walking Intention Based on Dynamical Movement Primitives," *IEEE TCDS*, vol. 13, no. 1, pp. 67–79, 2020.
- [5] L. M. Castano and A. B. Flatau, "Smart fabric sensors and e-textile technologies: a review," *Smart Materials and structures*, vol. 23, no. 5, p. 053001, 2014.
- [6] K. Yang, B. Isaia, L. J. Brown, and S. Beeby, "E-textiles for healthy ageing," *Sensors*, vol. 19, no. 20, p. 4463, 2019.
- [7] S. Qiu, H. Zhao, N. Jiang, *et al.*, "Sensor network oriented human motion capture via wearable intelligent system," *International Journal of Intelligent Systems*, vol. 37, no. 2, pp. 1646–1673, 2022.
- [8] O. Banos, M. A. Toth, M. Damas, H. Pomares, and I. Rojas, "Dealing with the effects of sensor displacement in wearable activity recognition," *Sensors*, vol. 14, no. 6, pp. 9995–10023, 2014.
- [9] L. Li, W. Au, Y. Li, K. Wan, W. Chung, and K. Wong, "A Novel Design Method for an Intelligent Clothing Based on Garment Design and Knitting Technology," *Textile Research Journal*, vol. 79, no. 18, pp. 1670–1679, 2009.
- [10] B. Michael and M. Howard, "Eliminating motion artifacts from fabric-mounted wearable sensors," in *2014 Humanoids*, IEEE, 2014, pp. 868–873.
- [11] B. Michael and M. Howard, "Learning Predictive Movement Models From Fabric-Mounted Wearable Sensors," *IEEE TNSRE*, vol. 24, no. 12, pp. 1395–1404, 2015.
- [12] M. Lorenz, G. Bleser, T. Akiyama, T. Niikura, D. Stricker, and B. Taetz, "Towards Artefact Aware Human Motion Capture using Inertial Sensors Integrated into Loose Clothing," in *2022 ICRA*, IEEE, 2022, pp. 1682–1688.
- [13] B. Michael and M. Howard, "Activity recognition with wearable sensors on loose clothing," *Plos one*, vol. 12, no. 10, e0184642, 2017.
- [14] U. Jayasinghe, W. S. Harwin, and F. Hwang, "Comparing Clothing-Mounted Sensors with Wearable Sensors for Movement Analysis and Activity Classification," *Sensors*, vol. 20, no. 1, p. 82, 2019.
- [15] U. Jayasinghe, F. Hwang, and W. S. Harwin, "Comparing Loose Clothing-Mounted Sensors with Body-Mounted Sensors in the Analysis of Walking," *Sensors*, vol. 22, no. 17, p. 6605, 2022.
- [16] U. Jayasinghe, B. Janko, F. Hwang, and W. S. Harwin, "Classification of static postures with wearable sensors mounted on loose clothing," *Scientific Reports*, vol. 13, no. 1, p. 131, 2023.
- [17] T. Shen, I. Di Giulio, and M. Howard, "A Probabilistic Model of Activity Recognition with Loose Clothing," in *2023 ICRA*, IEEE, 2023, pp. 12659–12664.
- [18] I. Visser, "Seven things to remember about hidden Markov models: A tutorial on Markovian models for time series," *Journal of Mathematical Psychology*, vol. 55, no. 6, pp. 403–415, 2011.
- [19] X. S. Papageorgiou, G. Chalvatzaki, C. S. Tzafestas, and P. Maragos, "Hidden markov modeling of human normal gait using laser range finder for a mobility assistance robot," in *2014 ICRA*, IEEE, 2014, pp. 482–487.
- [20] L. R. Rabiner, B.-H. Juang, S. E. Levinson, and M. M. Sondhi, "Some Properties of Continuous Hidden Markov Model Representations," *AT&T technical journal*, vol. 64, no. 6, pp. 1251–1270, 1985.
- [21] Y. C. Subakan, J. Traa, P. Smaragdus, and D. Hsu, "Method of moments learning for left-to-right Hidden Markov models," in *2015 WASPAA*, IEEE, 2015, pp. 1–5.
- [22] L. R. Rabiner, "A Tutorial on Hidden Markov Models and Selected Applications in Speech Recognition," *Proceedings of the IEEE*, vol. 77, no. 2, pp. 257–286, 1989.
- [23] M. Bicego, V. Murino, and M. A. Figueiredo, "Similarity-based classification of sequences using hidden Markov models," *Pattern Recognition*, vol. 37, no. 12, pp. 2281–2291, 2004.
- [24] F. Topsoe, "Some inequalities for information divergence and related measures of discrimination," *IEEE Transactions on information theory*, vol. 46, no. 4, pp. 1602–1609, 2000.
- [25] F. Porikli, "Trajectory Distance Metric Using Hidden Markov Model Based Representation," in *IEEE European Conference on Computer Vision, PETS Workshop*, vol. 3, 2004.
- [26] S. Pitou, F. Wu, A. Shafti, B. Michael, R. Stopforth, and M. Howard, "Embroidered Electrodes for Control of Affordable Myoelectric Prostheses," in *2018 ICRA*, IEEE, 2018, pp. 1812–1817.
- [27] S. Li, P. Zheng, S. Pang, X. V. Wang, and L. Wang, "Self-organising multiple human-robot collaboration: A temporal subgraph reasoning-based method," *Journal of Manufacturing Systems*, vol. 68, pp. 304–312, 2023.
- [28] Y. Chen, Y. Luo, C. Yang, *et al.*, "Human mobile robot interaction in the retail environment," *Scientific Data*, vol. 9, no. 1, p. 673, 2022.